



## **Comparison of AISC 360 and Eurocode 3 lateral-torsional and flange local buckling predictions to results from a comprehensive experimental database for rolled I-section members**

Aakash Reddy Eetikala<sup>1</sup>, Donald W. White<sup>2</sup>, Ryan J. Sherman<sup>3</sup>

### **Abstract**

Various prior efforts have quantified the accuracy of the ANSI/AISC 360 and the Eurocode 3 (EC3) lateral-torsional buckling (LTB) resistance predictions for rolled I-section members versus experimental data. This paper assesses the AISC 360-22 and the second-generation EC3 predictions relative to a comprehensive database of determinate rolled I-section beam LTB and flange local buckling (FLB) experimental tests. In addition, the predictions by newly proposed general-purpose AISC 360 I-section member provisions are scrutinized. Both uniform bending and moment gradient tests are considered. All the studies are based on rigorous elastic LTB solutions from thin-walled open-section beam theory as the underlying calculation, considering the physical tests' load and displacement boundary conditions. The results show that the newly proposed general-purpose AISC provisions provide minor improvements relative to the AISC 360-22 provisions for rolled I-shapes, consistent with substantive improvements demonstrated in recent research for general built-up I-section members. Meanwhile, the EC3 provisions tend to provide a conservative characterization of the mean flexural resistances.

### **1. Introduction**

Experimental investigations have played a significant role in furthering the understanding and the development of modern design standards for lateral torsional buckling (LTB) of I-section members. The AISC 360 Specification provisions for the flexural design of I-section members (AISC 2022) are based mainly on lateral-torsional buckling (LTB) experimental test data (Galambos 2004; White 2008; White and Jung 2008; White and Kim 2008). European efforts to quantify the LTB resistance of I-section members in flexure have also included substantive evaluations of experimental data, e.g., (Greiner and Kaim 2001); however, the Eurocode 3 (EC3) developments have emphasized the results from finite element analysis (FEA) simulation, i.e., geometrically and materially nonlinear analyses with imperfections (GMNIA) (Greiner et al. 2000; Taras 2008; Taras and Greiner 2010; Knobloch et al. 2020)

---

<sup>1</sup> Graduate Research Assistant, Georgia Institute of Technology, <aetikala3@gatech.edu>

<sup>2</sup> Professor, Georgia Institute of Technology, <dwhite@ce.gatech.edu>

<sup>3</sup> Assistant Professor, Georgia Institute of Technology, <ryan.sherman@ce.gatech.edu>

Recently, AISC Technical Committee 4 has developed a new Section F3 of the AISC 360 Specification, under consideration for the AISC 360-27 standard, providing substantial improvements in accuracy and ease-of-use for the design of general rolled and built-up I-section members. If approved, the new Section F3 provisions consolidate the prior AISC 360 Sections F3, F4, and F5 into one set of unified provisions applicable to all types of I-section members. The AISC 360-22 Section F2 provisions will be retained, but only for the design of compact rolled I-section members. The flange local buckling (FLB) resistance will be calculated using the new Section F3 for rolled I-section members with noncompact flanges. In other recent developments, the second-generation Eurocode 3 (CEN 2022) has refined its buckling calculations based on the research by Taras (2008) and Taras and Greiner (2010), reducing the conservatism of the first-generation Eurocode 3 rules in specific cases.

As discussed in Chapter 5 of the SSRC Guide to Stability Design Criteria for Metal Structures (Ziemian 2010), the characterization of the nominal LTB resistance of rolled I-section members can differ by as much as a factor of 2.0 between prominent design standards. Figures 1 and 2 are an updated version of the above-mentioned figure from the SSRC Guide, showing nominal LTB strength predictions for Grade 50 W27x84 beams in uniform bending with fork end conditions, and members in three-point bending with lateral bracing at the ends and at the midspan of the members ( $K = 1.0$ ,  $C_b = 1.75$ ), respectively. These figures show the LTB strength curves from AISC 360-22 Section F2, a newly proposed AISC 360 Section F3, and the second-generation EC3 (CEN 2022) Section 8.3.2.3(2) and 8.3.2.3(3) rules. EC3 Sections 8.3.2.3(2) and 8.3.2.3(3) give essentially the same results for uniform bending of the W27x84 members. The differences in the strength characterization for this fundamental design case are smaller than demonstrated for the previous standards by Ziemian (2010); however, the differences are still quite stark.

The discrepancies in the strength predictions by the design codes are more prominent for the beams subjected to moment gradient, i.e., non-constant moment along the unbraced length. One can observe that a length  $L_b = 21.75$  ft, the AISC 360-22 Section F2 provisions indicate a flexural resistance equal to the plastic moment  $M_p$ . However, at this same length, the general-case EC3 8.3.2.3(2) provisions indicate a capacity of only  $0.597M_p$ . The second-generation EC3 Section 8.3.2.3(3) rules, which apply to doubly-symmetric sections with fork boundary conditions at both ends, provide a larger capacity prediction of  $0.697M_p$  at this length. The version of the new AISC Section F3 provisions considered in this paper suggests a slightly more conservative prediction for the uniform bending case in Fig. 1, and a reduced strength at the knee of the AISC 360-22 Section F2 curve (at  $L_b = 21.75$  ft) of  $0.877M_p$  in Fig. 2.

The improvements for general built-up I-section members provided by the new AISC 360 Section F3 are highlighted by Phillips et al. (2024a and b), Slein et al. (2024), and White and Vaszilievits-Sömjén (2025). This paper focuses on the most recent AISC 360 and EC3 predictions relative to the experimental data for rolled I-section members. The predictions by the current AISC 360 Section F2, the newly proposed AISC 360 Section F3, and the second-generation EC3 rules are scrutinized, emphasizing the plastic (plateau strength) and inelastic LTB predictions. Both uniform bending and moment gradient experimental test results are considered. All the studies are based on rigorous elastic LTB solutions from thin-walled open-section beam theory for the underlying elastic buckling stress calculation, using models that replicate the load and displacement boundary conditions from the physical tests.

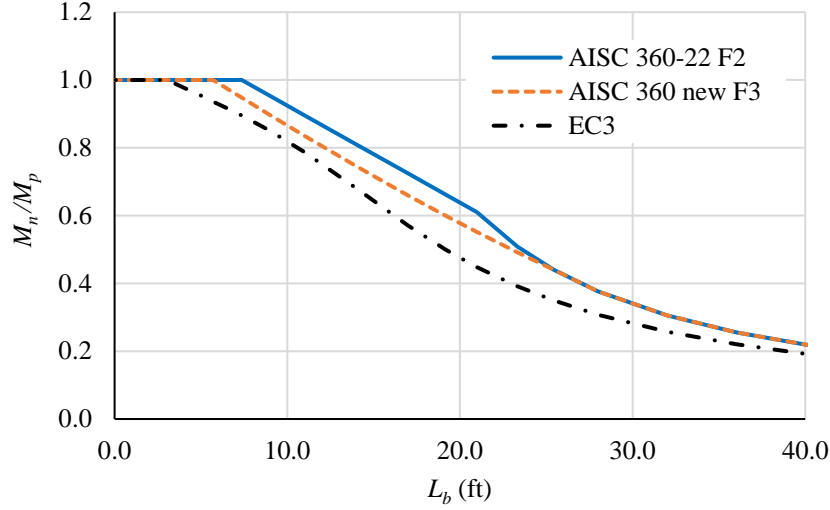


Figure 1: Predicted nominal LTB resistances in uniform bending for Grade 50 W27x84 beams with fork end conditions ( $K = 1.0$ ,  $C_b = 1.0$ )

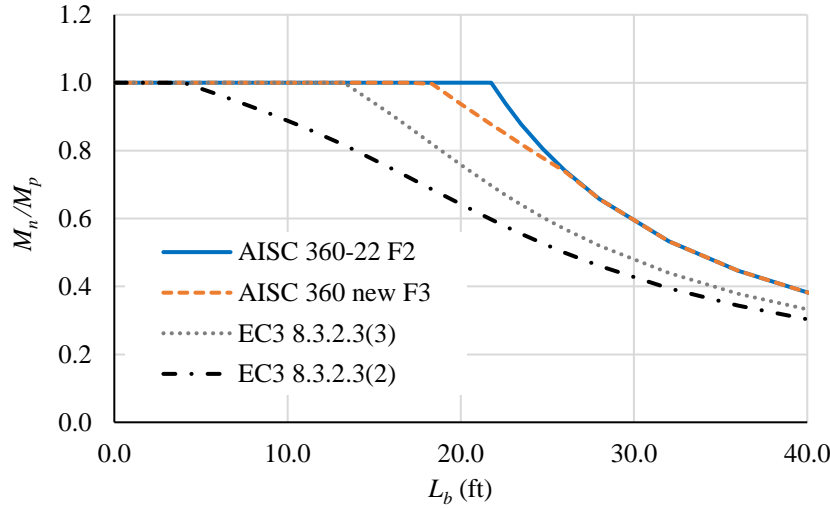


Figure 2: Predicted nominal LTB resistances for three-point bending of Grade 50 W27x84 beams with fork end conditions ( $K = 1.0$ ,  $C_b = 1.75$ )

## 2. Overview of AISC 360 and Eurocode 3 (EC3) Strength Calculations

The following sections provide an overview of the AISC 360 Section F2, the newly proposed AISC 360 Section F3, and the second-generation EC3 strength calculations evaluated in this paper.

### 2.1 Calculation of the LTB strength using AISC 360-22 Section F2

Figure 3 illustrates the AISC 360-22 Section F2 calculation of the LTB resistance for members subjected to uniform bending and moment gradient loading. The dashed grey line in the figure illustrates the LTB resistance for uniform bending, while the heavier dark solid line illustrates the LTB strength curve for a representative moment gradient case. The moment gradient curve is obtained by scaling the uniform bending curve by the moment gradient factor,  $C_b$ , and capping the increased strength by the plateau resistance.

The LTB strength curve for uniform bending consists of three distinct regions:

- The **plateau region**, corresponding to effective unbraced lengths  $KL_b \leq L_p$ , within which the nominal flexural resistance is the plastic moment,  $M_p$ , and where  $L_p$  is termed the compact bracing limit.
- The **inelastic LTB region**, defined for  $L_p < KL_b \leq L_r$ , where  $L_r$  is termed the noncompact LTB limit. In the inelastic LTB region, the strength is linearly interpolated between Anchor Point 1 ( $L_p, M_p$ ) and Anchor Point 2 ( $L_r, M_L$ ), where  $M_L = 0.7F_y S_x$  is the moment level above which the influence of inelasticity is considered in the LTB strength characterization. The length  $L_r$  is the value of  $KL_b$  at which the theoretical elastic LTB resistance equals  $M_L$ .
- The **elastic region**, defined for  $KL_b > L_r$ , where the LTB strength is taken as the theoretical elastic LTB resistance of the member.

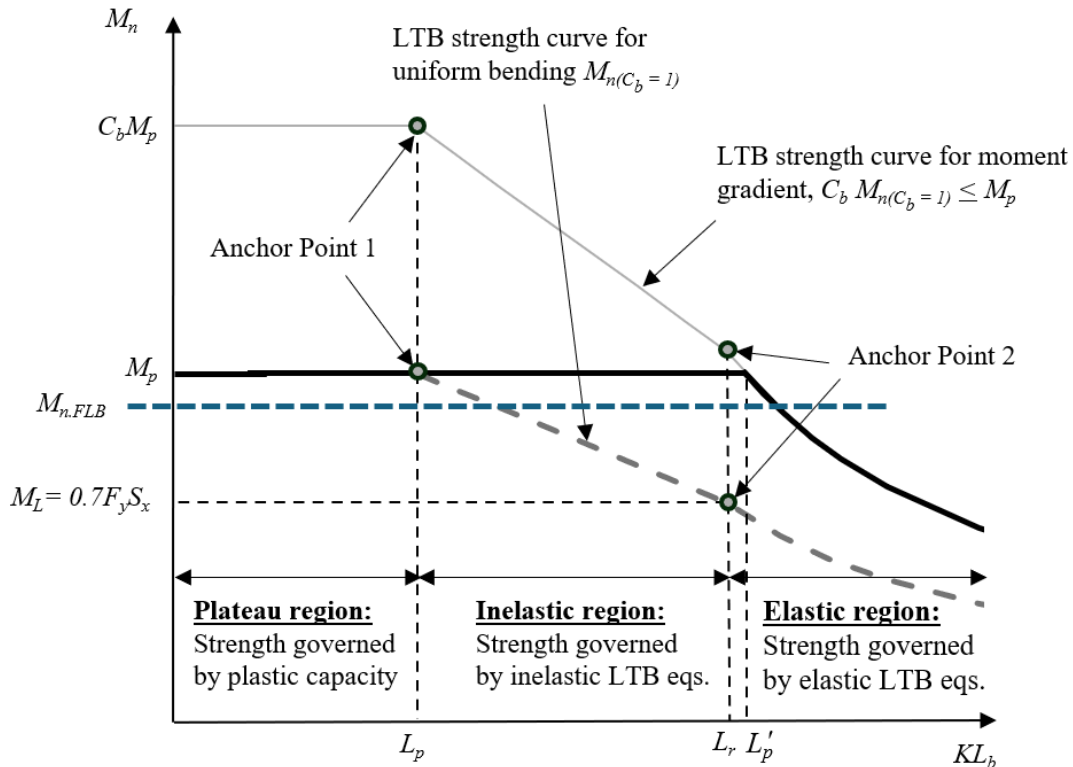


Figure 3: AISC 360-22 Section F2 LTB strength curves for rolled I-section members

The AISC Specification equations are written in terms of the unbraced length,  $L_b$ ; however, the Commentary explains that an effective length,  $KL_b$ , may be employed to calculate the resistance accounting for the end restraint conditions on the unbraced length. Also, although engineers often interpret that  $M_L = 0.7F_y S_x$  implies initial flange residual stresses of  $0.3F_y$ , the effects of the onset of yielding on the LTB resistance are influenced significantly by amplified compression flange lateral bending as the LTB strength limit state is approached for unbraced lengths near the elastic-to-inelastic LTB transition. Therefore, inferring  $0.3F_y$  residual stress from  $M_L = 0.7F_y S_x$  is an overly simplistic interpretation of the physical behavior.

AISC 360-22 Section F2 defines an independent FLB strength calculation for members with a noncompact compression flange. The FLB strength is shown in Fig. 3 as an independent maximum strength limit smaller than  $M_p$ . For compact-flange sections, such as the W27x84 members in

Figs. 1 and 2, the FLB limit state is not applicable, or it can be said that the FLB resistance is equal to the plateau strength,  $M_p$ . The FLB reduction relative to the maximum plateau strength  $M_p$  is typically small for rolled I-section members with noncompact flanges. In the new AISC 360 provisions under consideration for the 2027 Specification cycle, the predicted FLB resistance for noncompact flange members is increased slightly relative to the AISC 360-22 calculation, recognizing postbuckling strength contributions. In the present paper, both compact and noncompact flange members are included in the experimental test data. For the members with noncompact compression flanges, the FLB resistance is calculated in all cases using the new Section F3 provisions.

As noted above, the AISC 360-22 Section F2 accounts for the effects of moment gradient by scaling its uniform bending LTB strength curve by the moment gradient factor,  $C_b$ , but applying the plateau strength,  $M_p$ , as a maximum cap on the LTB resistance. The parameter  $C_b$  is derived as a scale factor on the elastic buckling resistance in uniform bending, quantifying the increase in the elastic LTB resistance due to a moment gradient. However, in the AISC Section F2 approach, elastically-derived  $C_b$  equations are applied to the uniform bending strength curve regardless of whether the moment levels are larger than the moment  $M_L$ . At moment levels larger than  $M_L$ , one would expect the onset of yielding to occur. Therefore, strictly speaking, the scaling of the uniform bending strength curve by  $C_b$  should not be valid for moment levels larger than  $M_L$ .

For instance, given a sufficient value for  $C_b$ , the AISC Section F2 approach scales the elastic LTB strength at Anchor Point 2 up to  $M_p$  without accounting for any reductions in the LTB resistance due to inelasticity. This is the case for the W27x84 examples shown in Figs. 1 and 2, where  $M_{n,FLB} = M_p$ . Figure 4 illustrates the specific behavior of the curves for this situation. Given the scaling of the uniform bending strength curve by  $C_b$ , the AISC 360 Section F2 approach suggests that the moment gradient effects completely remove any inelastic buckling range for this problem. The AISC 360 Section F2 indicates that the W27x84 LTB strength is the elastic LTB resistance all the way up to the point where the elastic LTB curve intersects the plateau at  $M_p$ .

The seminal paper by Yura et al. (1978), which recommended the application of  $C_b$  as shown in Fig. 3, addressed the above concern and explained that the corresponding approximation is acceptable. However, other researchers, such as Subramanian and White (2017), have raised concerns that the above approximation can overestimate the flexural strength, particularly when the maximum moment within the unbraced length is not at a braced point. Clearly, the EC3 Standard and the newly proposed AISC 360 Section F3 are less aggressive in their representation of the increased LTB strength due to moment gradient effects.

The  $C_b$  factor may be calculated using the following “quarter-point” equation proposed by Wong and Driver (2010), which is listed in the AISC 360-22 Commentary as Eq. C-F1-2b:

$$C_b = \frac{4M_{\max}}{\sqrt{M_{\max}^2 + 4M_A^2 + 7M_B^2 + 4M_C^2}} \quad (1)$$

In this equation,  $M_{\max}$  is the maximum moment within the unbraced length, and  $M_A$ ,  $M_B$ , and  $M_C$  are the moment values at quarter-point, mid-point, and three-quarter points within the unbraced length, respectively. Compared to the quarter-point Eq. F1-1 of the AISC 360-22 Specification, Equation 1 tends to provide slightly more accurate, larger, lower-bound predictions of rigorous

elastic LTB strengths for I-section member unbraced lengths with fork end conditions subjected to moment gradient. For instance, given an unbraced length with a linear moment diagram between zero at one end and maximum moment at the opposite end (such as the unbraced lengths corresponding to Fig. 2), Eq. 1 gives  $C_b = 1.75$  whereas Eq. F1-1 gives  $C_b = 1.67$  (5 % smaller).

Figure 3 denotes the unbraced length where the scaled LTB strength curve for moment gradient cases intersects the plateau strength by the symbol  $L_p'$ . For rolled wide-flange section members, the length  $L_p'$  may be written algebraically as

$$L_p' = L_p + \frac{(1 - 1/C_b)}{(1 - M_L/M_P)} (L_r - L_p) \quad (2)$$

for  $L_p' \leq L_r$ .

## 2.2 Calculation of the LTB strength for rolled sections using the newly proposed general-purpose AISC 360 Section F3

New AISC Section F3 provisions have been proposed to address the above problems for general noncompact and slender-web I-section members. The new Section F3 provisions are developed such that, in the limit that the web slenderness  $\lambda_w$  is less than or equal to  $0.7\lambda_{pw}$ , comparable predictions are obtained to those from Section F2. Moreover, the strength curve is written in terms of a normalized LTB slenderness instead of the unbraced length. The normalized LTB slenderness is defined as follows:

$$\lambda_{LT} = \sqrt{\frac{F_{yc}}{F_{cr}}} \quad (3)$$

where  $F_{cr}$  is the elastic LTB stress, equal to the elastic LTB moment divided by the elastic section modulus to the compression flange,  $M_{cr}/S_{xc}$ . For uniform bending of rolled wide-flange members, which have compact webs, the LTB strength curve is essentially the same as that from Section F2 if  $M_L$  is taken equal to  $0.7F_y$  and if the value of  $\lambda_{LT}$  at the end of the plateau region is taken approximately as 0.45. However, for general built-up I-section members, Section F3 defines the moment at the elastic-to-inelastic LTB transition as

$$M_L = 0.5F_y S_{xc} = 0.5M_{yc} \quad (4)$$

and, for uniform bending, it defines the value of the normalized slenderness at the end of the LTB strength plateau as

$$\lambda_{pLT} = 0.35 \quad (5)$$

The subsequent data analysis presented in this paper suggests that Eqs. 4 and 5 accurately characterize the experimental LTB strength data for rolled I-section members subjected to uniform bending. In addition, the elastic-to-inelastic LTB transition occurs at

$$\lambda_{rLT} = \sqrt{M_{yc}/M_L} = \sqrt{1/0.5} = 1.41 \quad (6)$$

in terms of the normalized LTB slenderness,  $\lambda_{LT}$ . The dashed grey curve in Fig. 4 shows the resulting LTB strength curve for uniform bending.

For moment gradient cases, the newly proposed AISC 360 Section F3 always considers the elastic-to-inelastic LTB transition as the moment level  $M_L$ . Also, for slender web members, Phillips et al. (2024a) and others have shown that Eq. 5 is the appropriate value for  $\lambda_{pLT}$ . However, for rolled wide-flange members having compact webs and other similar built-up section members, the version of the Section F3 provisions considered in this paper parallels the increase in the plateau length given by Eq. 2, but with a cap on the corresponding  $\lambda_{pLT}'$  of 0.8, i.e.,

$$\lambda_{pLT}' = \frac{1}{\sqrt{C_b}} \left[ 0.35 + \frac{1 - 1/C_b}{1 - M_L/M_p} (\lambda_{rLT} - 0.35) \right] \leq 0.8 \quad (7)$$

Substituting the result from Eq. 6 into Eq. 7, the following is obtained for rolled I-section members:

$$\lambda_{pLT}' = \frac{1}{\sqrt{C_b}} \left[ 0.35 + 1.06 \frac{1 - 1/C_b}{1 - M_L/M_p} \right] \leq 0.8 \quad (8)$$

It should be noted that the cap on  $\lambda_{pLT}'$  of 0.8 in the above equation is always smaller than  $\lambda_{rLT}$ . This cap restricts the increase in the plateau length based on the evaluation of the available experimental test data, and is the same as the cap recommended by Phillips et al. (2024a) and White and Vaszilievits-Sömjén (2025) for built-up I-section members.

Figure 4 illustrates how Eq. 8 works for moment gradient cases. For larger values of  $C_b$ , the linear transition between Anchor Point 2 ( $\lambda_{rLT}$ ,  $M_L$ ) and Anchor Point 1 ( $\lambda_{pLT}$ ,  $M_p$ ) can give values larger than the elastic LTB resistance. Therefore, in the transition between Anchor Points 1 and 2, the LTB resistance is taken as the smaller of the values from the linear interpolation between the anchor points and the elastic LTB resistance. The resulting behavior from this calculation mimics the behavior of the AISC 360 Section F2 LTB strength curves to some extent in that the moment level at the onset of yielding effects is increased. However, the increase is limited by Anchor Point 2 always being at ( $\lambda_{rLT}$ ,  $M_L$ ) and by  $\lambda_{pLT}'$  being capped at 0.8.

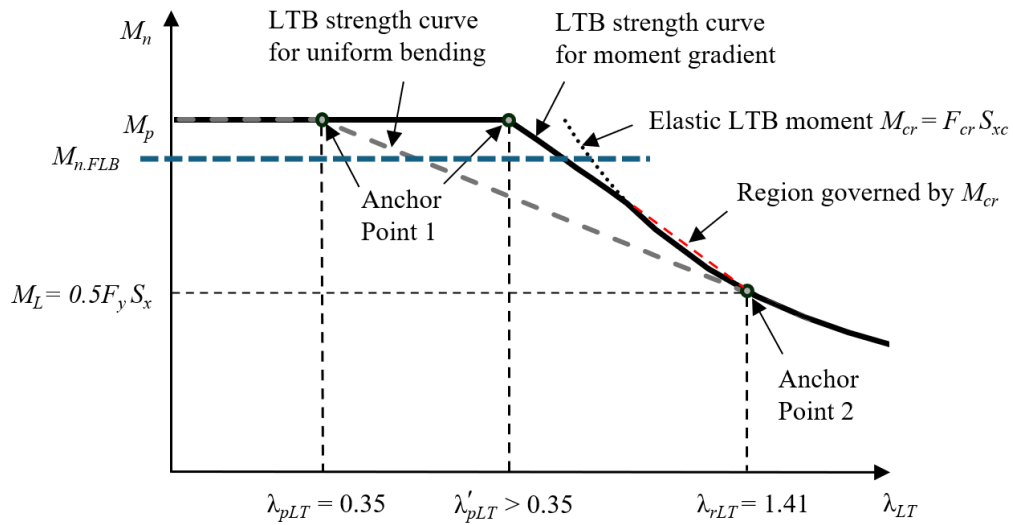


Figure 4: Newly proposed AISC Section F3 LTB strength curves for rolled I-section members

Lastly, for noncompact flange I-shapes, the FLB resistance is implemented as the same independent strength limit,  $M_{n.FLB} \leq M_p$ , as discussed previously in the context of AISC 360 Section F2. A horizontal dashed line is again shown in Fig. 4 to represent the FLB strength cap.

It should be noted that the current Ballot 2 version of Section F3 uses a simpler expression for  $\lambda_{pLT'}$  that approximates the behavior of Eq. 8. Equation 8 is recommended since it parallels the behavior of  $L_p'$  in Eq. 2, which is the behavior for the end of the plateau in Section F2, but with a cap on  $\lambda_{pLT'}$  of 0.8.

### 2.3 Calculation of LTB strength for rolled sections using the second-generation EC3

EC3 (CEN 2022) defines a plateau for its LTB strength curves that works effectively as the member cross-section strength in the limit of a small unbraced length. For cross-sections that satisfy the Class 1 or Class 2 requirements, the plateau resistance is expressed as

$$M_{Rk} = M_p \quad (9)$$

For Grade 50 steels, all the ASTM A6 rolled wide-flange (W) sections have Class 1 or Class 2 webs. However, a small subset of rolled wide-flange sections composed of Grade 50 steels have Class 3 flanges. In these cases, the plateau strength, denoted by the symbol  $M_{Rk}$ , is smaller than the plastic moment. None of the ASTM A6 W sections have Class 4 compression flanges for Grade 50 steel, where Winter's effective width model is employed to describe a postbuckled strength smaller than  $M_{yc}$ ; however, for higher strength steels, some W-sections have a Class 4 flange.

Once the cross-section strength has been determined, the EC3 LTB strength curves are generated as a function of the normalized slenderness parameter

$$\bar{\lambda}_{LT} = \sqrt{\frac{M_{Rk}}{M_{cr}}} \quad (10)$$

The nominal LTB resistance is then expressed as

$$M_n = \chi_{LT} M_{Rk} \quad (11)$$

where based on Section 8.3.2.3(2), which addresses general cases,

$$\chi_{LT} = \frac{1}{\phi + \sqrt{\phi^2 - \bar{\lambda}_{LT}^2}} \quad (12)$$

is an LTB reduction factor on the cross-section resistance. The parameter  $\phi$  in Eq. 12 depends on  $\bar{\lambda}_{LT}$  as well as an imperfection factor  $\alpha$  that defines the shape of the LTB strength curve. Two different imperfection factors are defined in EC3, giving the curves a and b illustrated in Fig. 5, which are applicable to sections with  $d/b_f \leq 2.0$  and  $d/b_f > 2.0$ , respectively. It should be noted that for both curves shown in Fig. 5, the length of the plateau corresponds to  $\bar{\lambda}_{LT} = 0.2$ . The corresponding value of  $\lambda_{LT}$  from Eq. 3 is typically about 4 to 7 percent smaller; the logic for the use of Eq. 3 in the AISC Section F3 provisions is that the onset of yielding leading to inelastic LTB is more strongly associated with  $F_y / F_{cr}$  than  $M_p / M_{cr}$ . Also, the EC3 strength curves only



approach the theoretical elastic LTB resistance asymptotically in the limit that  $\bar{\lambda}_{LT}$  becomes extremely large (e.g., see Figs. 1 and 2).

The provisions in the second-generation EC3 Section 8.3.2.3(3) provide an improved (larger) estimate of the LTB resistance in many situations by including additional terms that: (1) improve the Ayrton-Perry calibration regarding the imperfection factor, (2) help quantify the different buckling behavior of deep members with relatively thin cross-section elements versus shallow members with relatively stocky cross-section elements, and (3) implicitly recognize the beneficial effects of moment gradient, particularly the smaller spread of plasticity along the unbraced length compared to uniform bending tests. However, Section 8.3.2.3(3) is limited to doubly-symmetric members with fork boundary conditions at both ends. As such, in this paper, the Section 8.3.2.3(3) provisions are employed when calculating the strengths for a large number of three-point bending moment gradient test specimens; however, the general case provisions of Section 8.3.2.3(2) are employed to calculate the EC3 strengths for all the other tests considered in this study, since all the other tests have end restraint conditions. For uniform bending of many beam-type members, the Section 8.3.2.3(2) and (3) provisions essentially give the same strength prediction. This is the case for the W27x84 members in Fig. 1.

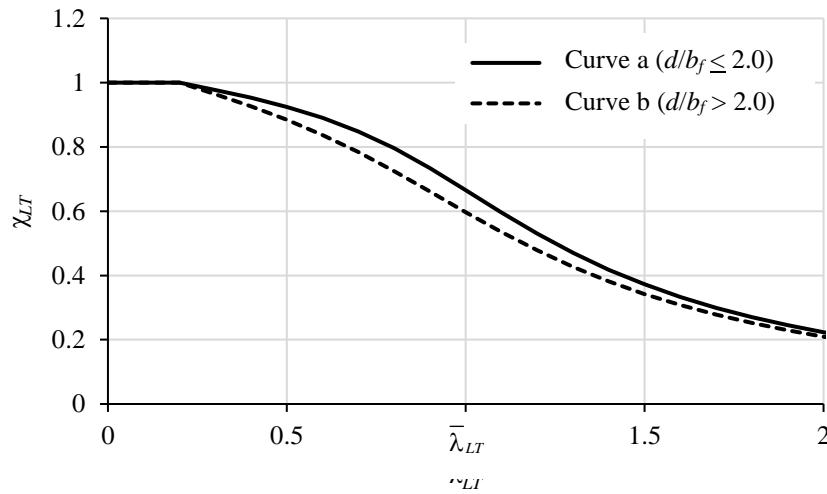


Figure 5: LTB curves for rolled sections defined by the EC3 provisions

### 3. Experimental Database for Rolled Sections

Previous studies (Fukumoto and Kubo 1977; Grenier and Kaim 2001; White and Kim 2008; White and Jung 2008; Subramanian et al. 2018) have developed experimental databases for rolled I-section members considering the available experimental data for both uniform bending and moment gradient cases. Building on the prior work, the current study collects and interrogates the experimental LTB and FLB tests and test results for rolled I-section members documented in the literature and evaluates the test strength predictions by the AISC and EC3 calculations discussed in Section 2. Tests governed by the AISC or EC3 modified plateau strengths associated with FLB, e.g.,  $M_{n,FLB}$  in Figs. 3 and 4, are included providing an assessment of the plateau strength predictions for both compact and noncompact flange rolled I-section members. Aside from the evaluation of the current AISC and EC3 calculations, the current study provides new data by using rigorous solutions from thin-walled open-section beam theory for the underlying elastic LTB

calculations in all cases, considering the physical tests' load and displacement boundary conditions. In addition, particular attention is given to the determination of the cross-section properties employed for the design calculations, given the measured dimensions and material strengths from the documentation of the prior tests. The following section discusses the specific selection and exclusion criteria for the experimental tests considered in this research.

### *3.1 Selection criteria and exclusions*

The current study is focused specifically on rolled I-section beam LTB and FLB experimental tests from the literature. Tests of built-up I-section members of any form, e.g., tests of rolled I-section members with channel caps, are not considered. Phillips et al. (2024a and b) and Slein et al. (2024) provide a comprehensive discussion of experimental test results for built-up three-plate welded I-section members; these results are not considered in this study. A large number of rolled I-section beam tests have been conducted in which transverse loads are applied to the member along its unbraced length. These tests generally require the consideration of load-height effects in the calculation of the elastic LTB resistance,  $M_{cr}$ , and/or in the calculation of the modifier,  $C_b$ . These types of tests are excluded from the current study to simplify the various considerations. All the tests considered in the current study have lateral and/or torsional bracing at each of the locations where load is applied. In addition, the emphasis in the current study is on unbraced lengths or normalized LTB slenderness values such that the strengths are close to or within the plastic and inelastic LTB ranges shown in Fig. 4. Galambos and Ravindra (1976) considered predictions for a large number of elastic LTB tests in their research.

Of the experimental LTB tests considered, a few tests are discarded for the following reasons:

- The specifics of the test boundary conditions are uncertain. For instance, in some situations, the researchers have documented uniform four-point bending LTB tests using similar sections reinforced with flange cover plates in adjacent end unbraced lengths and extending a short distance into the critical unbraced length, to deliver the moment to the critical unbraced length, but the specifics of the end cross-sections and the length of the extensions into the critical unbraced length are not provided. In other cases, uniform four-point bending tests have been conducted by applying transverse loads at an unspecified height to adjacent end overhangs of unspecified length to deliver the moment to the critical unbraced length. In all these types of situations, the tests are discarded from the database since the boundary conditions cannot be accurately quantified for the design strength calculations.
- Measured static yield strengths or yield strengths from coupon tests conducted at specified slow rates are not reported.

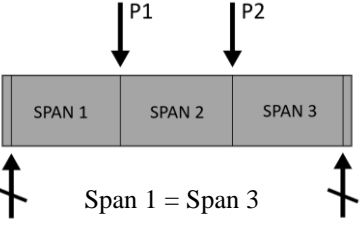
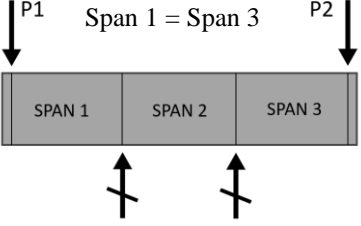
White and Jung (2008), White and Kim (2008), and Phillips et al. (2024a and b) discuss other general exclusion criteria for the broader range of built-up I-section member tests, but none of these additional criteria applied for the specific tests considered in the current study.

The following sections provide an overview of the uniform bending and moment gradient tests included in the study. Eetikala et al. (2025) provides the detailed information and data collected for all the subject tests.

### 3.2 Uniform moment tests

A total of 150 experimental tests from 14 studies were considered to build the experimental database of uniform moment tests in the current study. Table 1 summarizes the loading configurations, intermediate bracing conditions, number of tests, and references. As noted previously, all the tests considered in the current study have lateral and/or torsional bracing at each of the locations where load is applied. “Span 2” is the critical unbraced length in each of these tests.

Table 1. Summary of uniform moment experimental tests selected for the rolled I-section beam LTB/FLB database.

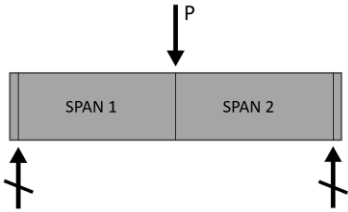
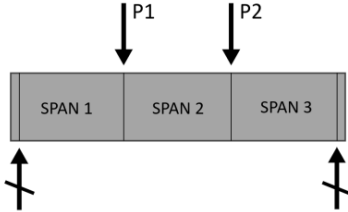
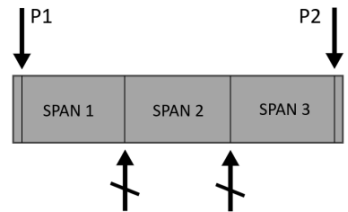
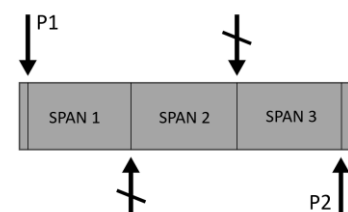
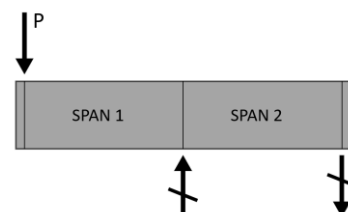
Loading Configuration	Number of Tests	Number of intermediate brace points*	Reference
	2	0	Driscoll and Beedle (1957)
	4	2	Prasad and Galambos (1963)
	5	1	McDermott (1969)
	3	0	Dux and Kitipornchai (1983)
	6	0	Wong-Chung and Kitipornchai (1987)
	5	1	
	4	0	Lee and Galambos (1962)
	14	0	Lee et al. (1964)
	6	0	Adams et al. (1964)
	7	0	Janss and Massonnet (1967)
	30	0	Dibley (1969)
	12	0	Dibley (1970)
	4	0	Suzuki and Ono (1970a)
	4	1	
	3	2	
	4	0	Wakabayashi et al. (1970)
	18	0	Udagawa et al (1973)
	13	1	
	6	2	

\* The intermediate brace points are located in the critical span, i.e., Span 2.

### 3.3 Moment gradient tests

A total of 84 experimental tests from 11 studies were considered for building the experimental database of moment gradient tests in the current study. Again, each load point is a braced point in these tests. Most of these experiments were three-point bending tests involving two unbraced lengths with  $K = 1.0$  and  $C_b = 1.75$  from Eq. 1. However, there are a few tests with different loadings corresponding to other  $C_b$  values, and one case with reverse-curvature loading. The following table summarizes the loading configurations, number of tests, and references.

Table 2. Summary of moment gradient experimental tests chosen for the rolled sections database

Loading Configuration		Number of Tests	Reference
	Span 1 = Span 2	1	Driscoll and Beedle (1957)
		18	Sawyer (1961)
		3	Adams et al. (1964)
		24	Lukey et al. (1969)*
		4	Suzuki and Ono (1970b)
		3	Dux and Kitipornchai (1983)
		4	Kemp (1986)
		5	Boeraeve et al. (1993)
		4	Kemp (1996)
	Span 1 = Span 3 $P1 \neq P2$	4	Kusuda et al. (1960)
		3	Dux and Kitipornchai (1983)
	Span 1 = Span 3 $P1 \neq P2$	1	Adams et al. (1964)
	Span 1 $\neq$ Span 3 $P1 \neq P2$	2	Janss and Massonnet (1967)
	Span 1 = Span 2 = Span 3 $P1 = P2$	1	Janss and Massonnet (1967)
	Span 1 = Span 2	7	Janss and Massonnet (1967)

\* Four of the Lukey et al. (1969) tests have one intermediate brace positioned in each of their two spans.

#### 4. Methodology

This section outlines the specific methodologies for the various design calculations employed in the current study.

##### 4.1 Calculation of section properties

All the strength calculations performed in this study are based on cross-section plate dimensions or detailed measured section properties specified within the reference documents. In some cases, the dimensions are reported in integer mm values, implying that the dimensions are only nominal values. This occurrence was not taken as a criterion to discard the test. All the “essential” tests for evaluation of the LTB strength curves, discussed subsequently, have detailed dimensional measurements and/or sufficient measured section properties such that unique plate dimensions could be determined.

All the strength calculations are based on measured static yield strengths or yield strengths from coupon tests conducted at specified slow rates. Where separate flange and web yield strengths are reported, the plastic moment  $M_p$  is calculated using the flange yield strength for the flanges and the web-to-flange fillet areas, and the web yield strength for the web. Many of the tests documented in the literature report only one measured yield strength. In this case, the single measured yield strength is employed for the calculations. A substantial number of the “essential” tests include separately measured flange and web yield strengths.

In addition, where specific information about the web-to-flange fillet areas is provided, the web-to-flange fillet areas are included in the section property calculations based on the specified radius of the fillets, or a circular radius of the fillets is calculated to match the specified cross-sectional areas including the web-to-flange fillets. Many of the rolled I-section tests from the literature do not include documentation of the cross-section web-to-flange fillet areas. In these cases, the web-to-flange fillet area implied by the difference between the sum of the plate areas and the total nominal cross-sectional area in the corresponding standard section property tables is employed to calculate the assumed radii of the web-to-flange fillets.

The specific calculation of the St. Venant torsions constant,  $J$ , is important. In the previous database studies by White and Jung (2008), White and Kim (2008), and Subramanian et al. (2018),  $J$  was calculated using the equation

$$J = \frac{ht_w^3}{3} + \frac{b_{fc}t_{fc}^3}{3} \left( 1 - 0.63 \frac{t_{fc}}{b_{fc}} \right) + \frac{b_{ft}t_{ft}^3}{3} \left( 1 - 0.63 \frac{t_{ft}}{b_{ft}} \right) \quad (13)$$

recommended by AASHTO (2024) and MBMA/AISC Design Guide 25 (White et al. 2021a) for built-up three-plate welded sections. Equation 13 provides a relatively conservative estimate of the St. Venant torsion constant neglecting the significant contribution from the web-to-flange junctures including the web-to-flange fillets. In this research, a rigorous analytical calculation of the St. Venant torsion constant is employed considering the specified web-to-flange fillet radii. Specifically, the calculation is made using the ConSteel (2025) software system. The values from ConSteel are checked using equations recommended by ElDarwish and Johnston (1965), which include the contribution of the web-to-flange fillet areas. The estimates from ElDarwish and Johnston are typically slightly smaller and within 10 percent of ConSteel values. In most cases the differences are only a few percent.

#### 4.2 Calculation and use of the elastic critical buckling moment $M_{cr}$

In this study, all the tests collected in the database are modeled with their specified geometry, and load and displacement boundary conditions, and the ConSteel (2025) software system is employed to determine the corresponding elastic critical buckling moment of the test,  $M_{cr}$ . The elastic buckling moments from ConSteel are verified using independent calculations from SABRE2 (White et al. 2021b) and considering rigorous benchmark analytical solutions.

For the newly proposed AISC Section F3 and the EC3 calculations,  $M_{cr}$  is substituted directly into the corresponding normalized slenderness Eqs. 3 and 10, respectively. Also, for the three-point bending moment gradient tests, effectively having fork end conditions and  $K = 1.0$ , the rigorous value for  $C_b$  is back-calculated by setting the result from the analytical equation for the elastic LTB resistance (e.g., AISC 326-22 Eq. F2-4) equal to  $M_{cr}$ . For all other tests, the moment gradient factor  $C_b$  is calculated from Eq. 1 and the rigorous value for the LTB effective length factor,  $K$ , is back-calculated by setting the result from the analytical equation for the elastic LTB resistance equal to  $M_{cr}$ . The Section F3 calculations then use the above  $C_b$  values in the calculation of  $\lambda_{pLT'}$  from Eq. 8. The  $K$  values are employed in plotting LTB strengths should one wish to plot the flexural resistance versus  $KL_b$ .

For the AISC 360 Section F2 provisions, the above  $C_b$  and  $KL_b$  values are employed in the AISC Section F2 equations.

#### 4.3 Estimation of reliability indices

The structural reliability in Load and Resistance Factor Design (LRFD) can be quantified by the probabilistically derived reliability index,  $\beta$ . Discussion of the background to and the calculation of the reliability index can be found in (Ellingwood et al. 1980; Ellingwood et al. 1982; Galambos et al. 1982; and Galambos 2004). The calculations in this study follow the detailed process outlined by White and Jung (2008).

The reliability index, based on an assumed log-normal distribution of the data and using the ASCE 7 (ASCE 2022) dead and live load combination factors of 1.2 and 1.6, can be expressed as:

$$\beta = \frac{1}{\sqrt{V_R^2 + V_Q^2}} \ln \left[ \frac{\bar{\rho}_R}{\phi_{LRFD}} \left( \frac{1.2 + 1.6 \left( \frac{L}{D} \right)}{\bar{\rho}_D + \bar{\rho}_L \left( \frac{L}{D} \right)} \right) \right] \quad (14)$$

where,  $V_R$  is the coefficient of variation (COV) of resistance effects,  $V_Q$  is the COV of the load effects,  $\bar{\rho}_D$  is the mean dead load bias factor,  $\bar{\rho}_L$  is the mean live load bias factor,  $\phi_{LRFD} = 0.9$  is the LRFD resistance factor or I-section member flexure, and  $L/D$  is taken as 3.0. Also,

$$\bar{\rho}_R = \bar{\rho}_M \bar{\rho}_G \bar{\rho}_P \quad (15)$$

and

$$V_R = \sqrt{V_M^2 + V_G^2 + V_P^2} \quad (16)$$

where,  $\bar{\rho}_M$ ,  $\bar{\rho}_G$ , and  $\bar{\rho}_P$  are the mean material, geometric, and professional bias factors.  $V_M$ ,  $V_G$ , and  $V_P$  are the COVs of the material, geometric, and professional bias factors. In this study, the parameters  $\bar{\rho}_M$ ,  $\bar{\rho}_G$ ,  $V_M$ , and  $V_G$  are taken the same as employed by Galambos (2004) and White and Jung (2008). The parameters  $\bar{\rho}_P$  and  $V_P$  are determined from the test data.

## 5. Results and Discussion

Figures 6 and 7 plot the professional factors,  $\rho_p = M_{test}/M_n$ , for the three sets of design provisions reviewed in Section 2 versus the normalized slenderness,  $\lambda_{LT}$ , for the uniform bending and moment gradient tests, respectively. Additionally, Tables 3 and 4 summarize the professional factor statistics and the resulting  $\beta$  values for several ranges of the normalized slenderness  $\lambda_{LT}$ , while Figs. 8 and 9 show the variation in the reliability indices versus  $\lambda_{LT}$  for uniform bending and moment gradient cases, respectively.

For cases typically governed by the plateau strength ( $\lambda_{LT} \leq 0.35$ ), all the provisions produce similar professional factors due to the strength being capped at  $M_p$  or  $M_{n,FLB}$ . For the uniform bending tests, the  $\beta$  values for these cases are slightly larger than the target of 2.6 originally specified for statically determinate beams in the first AISC LRFD Specification (Galambos 2004). The differences between the EC3 values and the AISC Section F2 or F3 values are due to the different FLB strength predictions in EC3. On average, the EC3 FLB strengths tend to be smaller than the AISC FLB strengths. However, in a few cases, the predicted EC3 FLB strength is slightly larger. This is due to the subtraction of the web thickness and web-to-flange fillet radius in the flange b/t checks in EC3.

The  $\rho_p$  values for the moment gradient tests for  $\lambda_{LT} \leq 0.35$  are, with one exception, all greater than 1.0 and they exhibit substantial dispersion (see Fig. 7). This behavior is due to the variable influence of strain hardening on the experimental strengths for small LTB slenderness, depending on the nature of the moment gradient and other factors. All the standards produce comparable results for these tests, with an estimated reliability index of 3.35 to 3.36 (see Fig. 9).

For unbraced lengths in uniform bending with normalized slenderness in the  $0.35 < \lambda_{LT} < 0.70$  range, the strength predictions from EC3 tend to be slightly conservative compared to the AISC strength predictions. Compared to AISC Section F3, the strength predictions from Section F2 have a slightly lower reliability index of 2.56. However, the slightly lower reliability index is not a concern for these cases. For moment gradient cases, both AISC provisions offer similar strength predictions whereas EC3 is more conservative.

For uniform bending specimens with larger normalized slenderness ( $\lambda_{LT} > 0.70$ ), which are typically governed by inelastic LTB, the AISC Section F2 gives reliability indices that are consistently slightly lower than the target of 2.6, while Section F3 provides reliability indices of 3.10 and 2.81 (see Fig. 8). Figure 6 shows that Section F2 gives professional factors mostly less than 1.0 for larger  $\lambda_{LT}$ . However, the EC3 results are significantly more conservative for these unbraced length ranges, with reliability index estimates of 3.17 for  $0.70 < \lambda_{LT} < 1.05$  and 3.84 for  $\lambda_{LT} > 1.05$ .

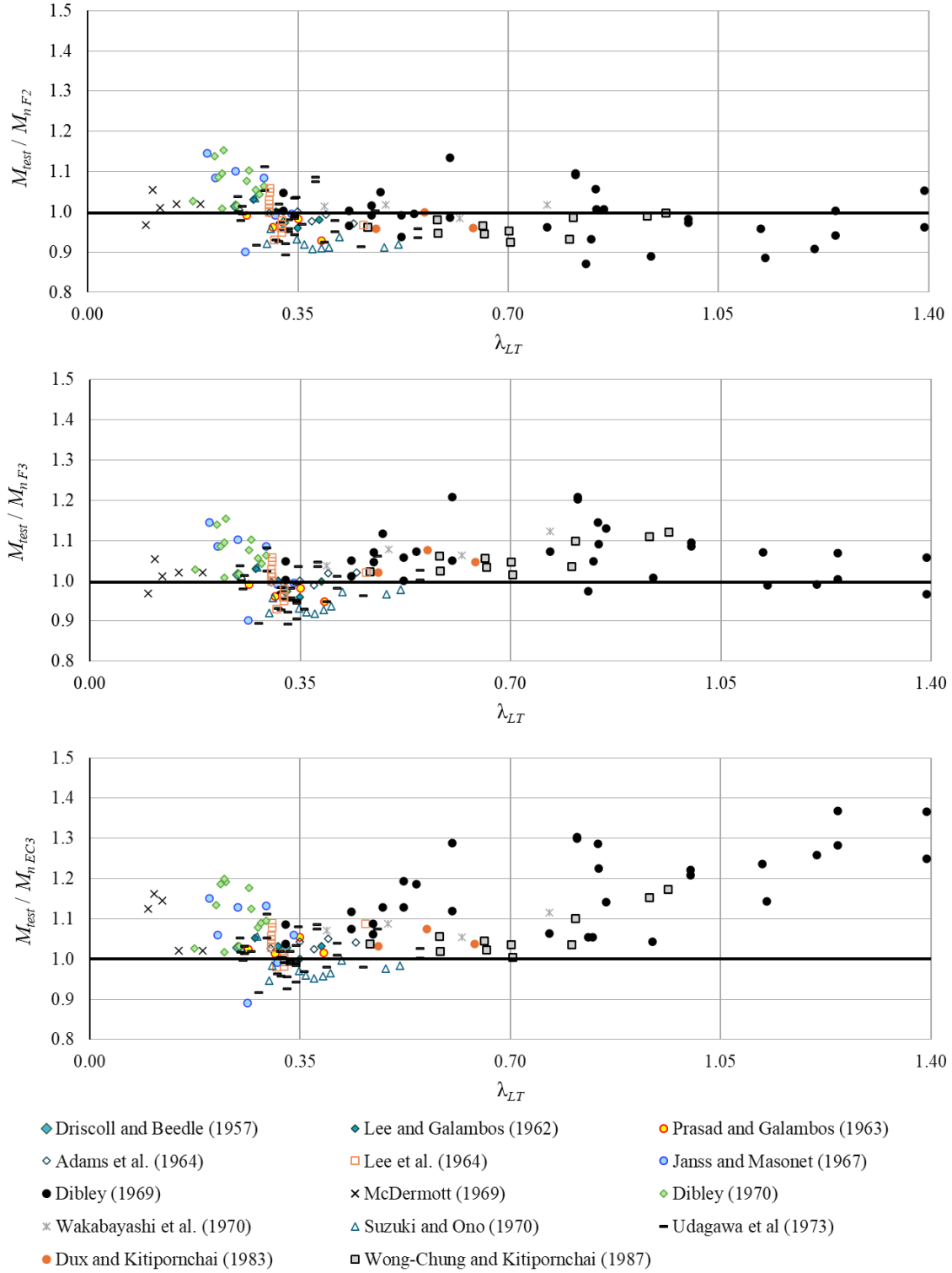


Figure 6: Professional factors versus normalized slenderness for uniform bending cases



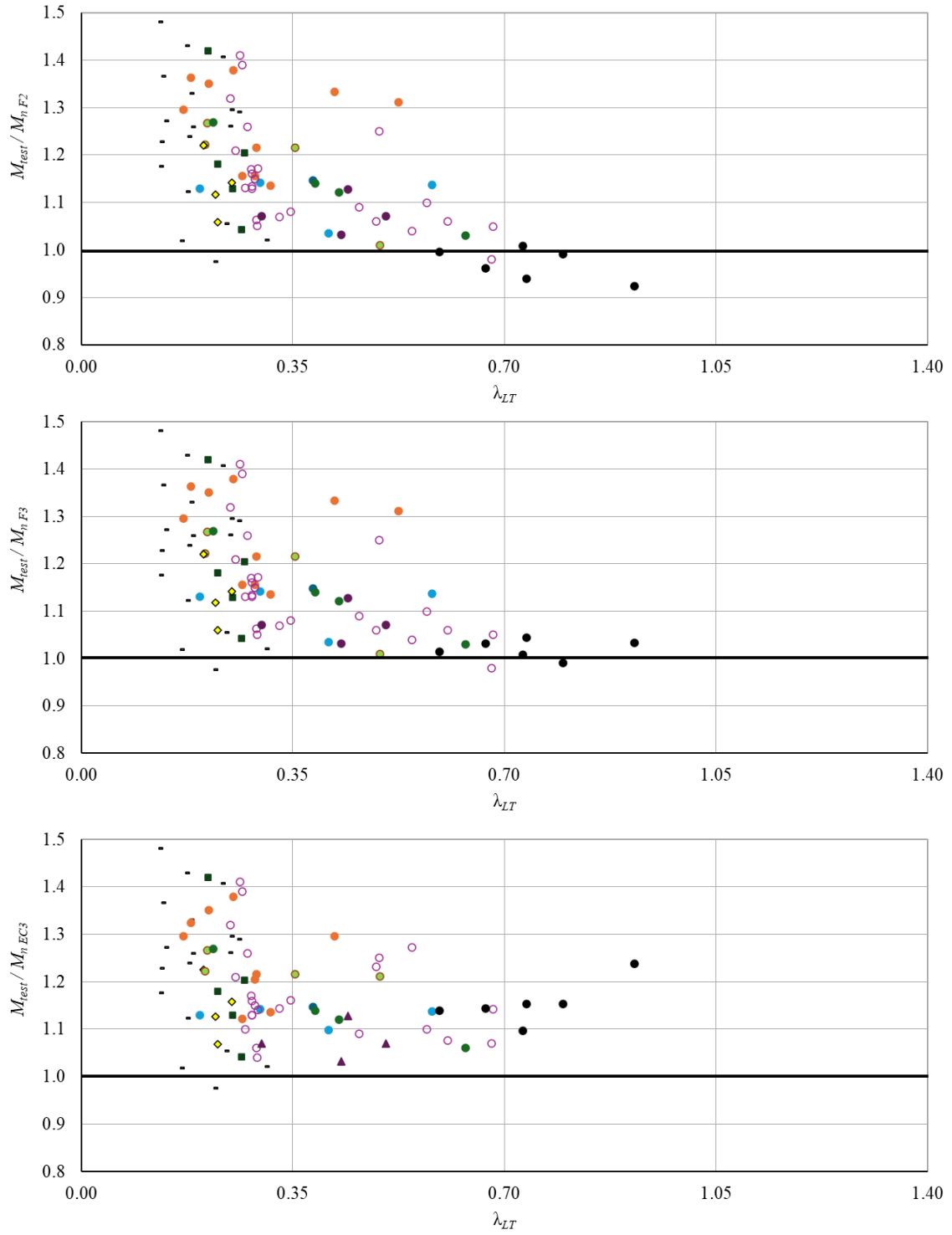


Figure 7: Professional factors versus normalized slenderness for moment gradient cases

Table 3. Summary of professional factor statistics and resulting reliability indices for uniform bending cases.

	$\lambda_{LT} \leq 0.35$			$0.35 < \lambda_{LT} \leq 0.70$			$0.70 < \lambda_{LT} \leq 1.05$			$\lambda_{LT} > 1.05$		
Statistical Values	$M_{test}/M_{nF2}$	$M_{test}/M_{nF3}$	$M_{test}/M_{nEC3}$	$M_{test}/M_{nF2}$	$M_{test}/M_{nF3}$	$M_{test}/M_{nEC3}$	$M_{test}/M_{nF2}$	$M_{test}/M_{nF3}$	$M_{test}/M_{nEC3}$	$M_{test}/M_{nF2}$	$M_{test}/M_{nF3}$	$M_{test}/M_{nEC3}$
N	81			44			18			7		
Mean	1.002	1.002	1.037	0.970	1.019	1.050	0.981	1.090	1.140	0.958	1.021	1.272
Median	0.997	0.997	1.026	0.966	1.021	1.041	0.984	1.093	1.129	0.958	1.003	1.258
Max	1.154	1.154	1.198	1.135	1.209	1.288	1.096	1.208	1.304	1.053	1.070	1.367
Min	0.892	0.892	0.890	0.907	0.918	0.951	0.870	0.974	1.005	0.885	0.966	1.144
Std Dev	0.057	0.057	0.064	0.045	0.057	0.068	0.061	0.063	0.099	0.057	0.043	0.078
COV	0.057	0.057	0.062	0.046	0.055	0.065	0.063	0.058	0.087	0.059	0.042	0.061
$\beta$	2.70	2.70	2.85	2.56	2.78	2.90	2.58	3.10	3.17	2.48	2.81	3.84

Table 4. Summary of professional factor statistics and resulting reliability indices for moment gradient cases.

	$\lambda_{LT} \leq 0.35$			$0.35 < \lambda_{LT} \leq 0.70$			$0.70 < \lambda_{LT} \leq 1.05$		
Statistical Values	$M_{test}/M_{nF2}$	$M_{test}/M_{nF3}$	$M_{test}/M_{nEC3}$	$M_{test}/M_{nF2}$	$M_{test}/M_{nF3}$	$M_{test}/M_{nEC3}$	$M_{test}/M_{nF2}$	$M_{test}/M_{nF3}$	$M_{test}/M_{nEC3}$
N	57			23			4		
Mean	1.207	1.207	1.209	1.100	1.104	1.161	0.965	1.019	1.161
Median	1.181	1.181	1.204	1.071	1.071	1.138	0.965	1.020	1.153
Max	1.481	1.481	1.481	1.334	1.334	1.538	1.008	1.044	1.238
Min	0.976	0.976	0.976	0.962	0.980	1.032	0.923	0.991	1.097
Std Dev	0.121	0.121	0.119	0.100	0.095	0.109	0.041	0.024	0.058
COV	0.101	0.101	0.099	0.091	0.086	0.093	0.042	0.023	0.050
$\beta$	3.35	3.35	3.36	2.99	3.03	3.22	2.54	2.83	3.42

For the longer unbraced lengths ( $\lambda_{LT} > 0.7$ ) in the moment gradient cases, the Chapter F3 recommended provisions provide a better characterization of results due to the  $\lambda_{pLT}'$  adjustment from Eq. 8, which provides more accurate predictions for the moment gradient tests from Dux and Kitipornchai (1983) in this slenderness range. As such, the recommended F3 provisions achieve a  $\beta$  of 2.83 as opposed to 2.54 from the Chapter F2 provisions.

The improved characterization by Section F3 for the moment gradient is illustrated by the plot shown in Fig. 9, where the strength curves corresponding to three of the three-point bending tests from Dux and Kitipornchai (1983), with  $K = 1$ ,  $C_b = 1.75$  from Eq. 1, and rigorous elastic LTB  $C_b$  values of 1.81 to 1.84, are shown. While the Chapter F2 strength curve overpredicts the capacity relative to the test data from the test with the largest  $L_b$  of 18.0 ft, Section F3 provides an accurate prediction. Although this illustration shows unconservatism in the AISC 360 Section F2 predictions for only one test, the trend in the  $M_{test}/M_{nF2}$  values shown in Fig. 7 is clearly decreasing  $M_{test}/M_{nF2} < 1.0$  with increasing  $\lambda_{LT}$  for the larger  $\lambda_{LT}$  values. The underlying reason for this trend is clear – AISC Section F2 tends to predict an LTB resistance equal to the theoretical elastic LTB strength all the way up to  $M_p$  or  $M_{nFLB}$  at these slenderness values when  $C_b$  is relatively large. One would expect that there should be some influence of the onset of yielding for these tests. The newly proposed AISC Section F3 rules give predictions that match this expectation.

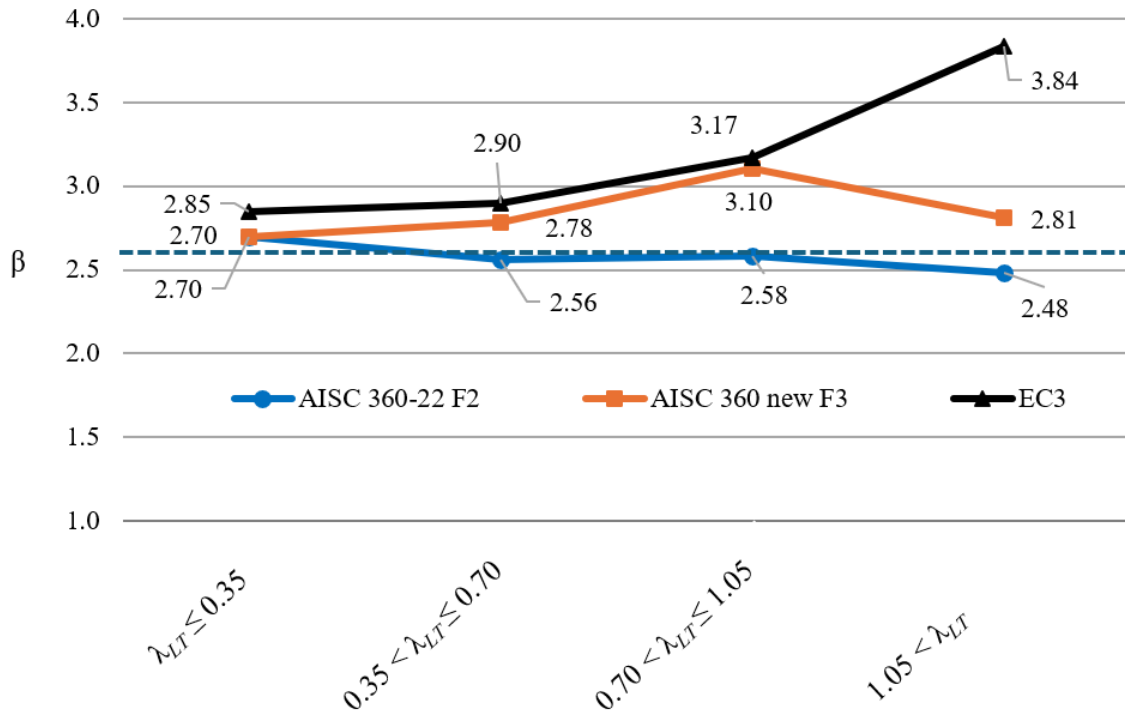


Figure 8: Estimated reliability indices versus  $\lambda_{LT}$  for members in uniform bending

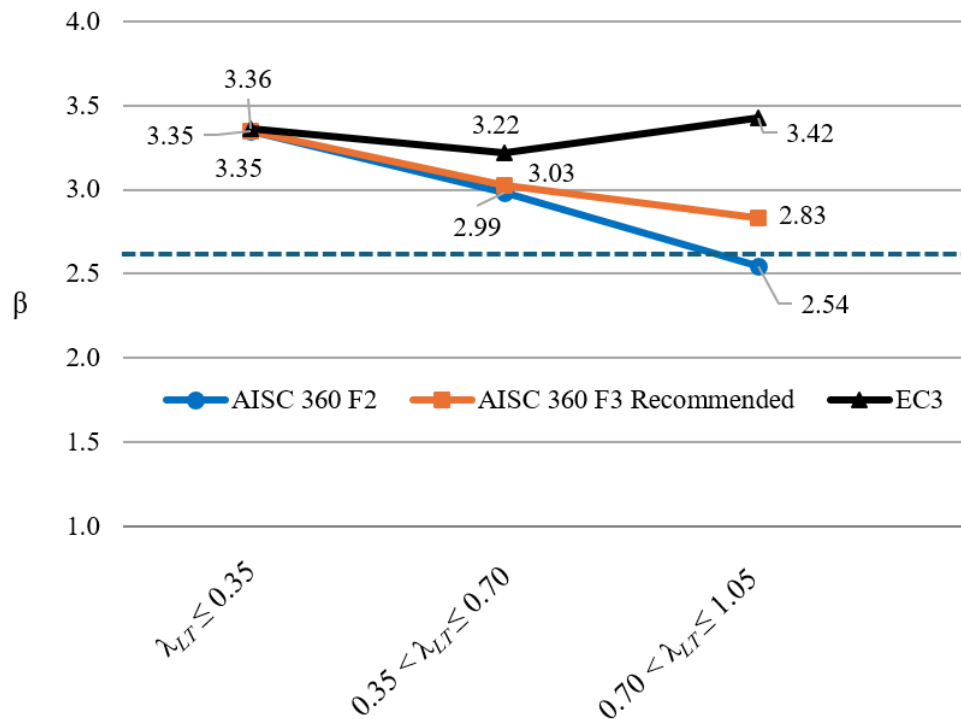


Figure 9: Estimated reliability indices versus  $\lambda_{LT}$  for members subjected to moment gradient

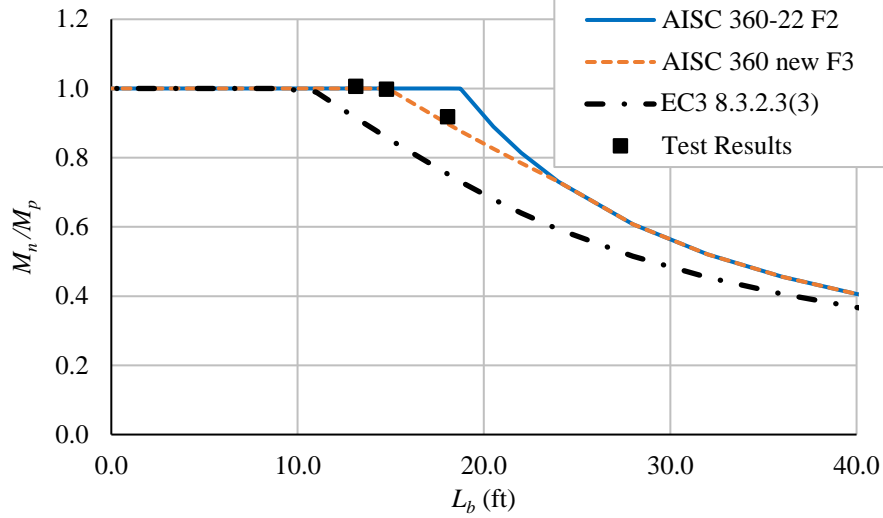


Figure 10: Comparison of Dux and Kitipornchai (1983) three-point bending test strengths with AISC 360-22 Section F2, the newly proposed AISC Section F3, and the EC3 8.3.2.3(3) predictions

One can observe that the EC3 predictions are significantly conservative relative to the moment gradient test data for the larger  $\lambda_{LT}$  values in Fig. 7. It is surmised that the conservatism of the EC3 rules is largely a product of a more detailed and cautious structural reliability assessment focusing predominantly on the data from GMNIA solutions with relatively damning assumed residual stress patterns (peak flange residual compressive stresses of  $0.3F_y$  or  $0.5F_y$ ) and relatively damning compression flange sweep (initial bow imperfections of parabolic shape with amplitude of  $L_b / 1000$ ) executed on isolated unbraced lengths having fork end conditions (Griener et al. 2000; Taras 2008; Taras and Greiner 2010; and Knobloch et al. 2020).

One can conclude that the Section F2 provisions perform marginally with respect to satisfying the target  $\beta$  of 2.6 at larger  $\lambda_{LT}$ . However, it should be noted there are only a few “essential” groups of tests that provide the data for these assessments. For uniform bending, the essential data mostly comes from Dibley (1969) and Wong-Chung and Kitipornchai (1987) (see Fig. 6). For uniform bending, the essential data for  $\lambda_{LT} > 0.70$  comes entirely from Dux and Kitipornchai (1983). The Dux and Kitipornchai (1983) and Wong-Chung and Kitipornchai (1987) papers have detailed cross-section dimensional measurements, including the web-to-flange fillet radius, and measured yield strengths for both the flanges and webs. The Dibley (1969) report provides detailed section property measurements sufficient to determine all the plate dimensions except the web-to-flange fillet radii, but no documentation of the web-to-flange fillet areas and only one reported value for the section yield strength.

Although not shown by the data presented, the proposed Section F3 provisions give results close to those of AISC 360-22 Section F2 for uniform bending (marginally satisfying the target  $\beta$  of 2.6) if the moment corresponding to the elastic-to-inelastic transition,  $M_L$  at Anchor Point 2, is increased to  $0.7M_{yc}$ . The current AISC 360-27 Ballot 2 specifies  $M_L = 0.7M_{yc}$  for rolled I-section members in its newly proposed Section F3. This change has little-to-no effect on the predictions for the moment gradient tests.

Structural stability researchers have investigated the LTB resistance of rolled I-section members over many years; however, there are no recent tests, and it would be useful to have additional new

data to confirm the above results. Furthermore, there is no data for highly slender beams subjected to moment gradient with  $\lambda_{LT} > 1.05$ . Given the decreasing trend with  $M_{test}/M_{nF2} < 1.0$  at the larger  $\lambda_{LT}$  values in Fig. 7 and the fact that there are no tests with  $C_b$  from Eq. 1 greater than 1.75, one can conclude that it would be prudent to limit the aggressive elimination of any inelastic LTB range by the AISC Section F2 calculations for high slenderness and high moment gradient. The newly-proposed Section F3 provisions accomplish this.

## 6. Conclusions

In this paper, a rolled I-section LTB/FLB experimental database consisting of 150 uniform bending and 84 moment gradient tests has been compiled and utilized for the assessment of strength predictions by the current AISC 360-22 Section F2 (AISC 2022), a newly proposed AISC 360 Section F3, and the second-generation Eurocode 3 (EC3) (CEN 2022) standards. It is observed that the strength predictions offered by the current Section F2 of AISC 360-22 marginally satisfy the established target  $\beta$  of 2.6 for statically determinate beam tests. The proposed Section F3 provisions provide comparable results to F2, slightly more conservative with minimum  $\beta$  values slightly larger than 2.6 if  $M_L$  is taken equal to  $0.5M_{yc}$ . The newly proposed Section F3 provisions offer an improved characterization of section capacity predictions specifically for moment gradient cases with larger LTB slenderness ( $\lambda_{LT} > 0.7$ ). These results are consistent with the substantial improvements provided by the Section F3 approach for more general built-up I-section members (Phillips et al. 2024a and b).

## References

- AASHTO (2024). *AASHTO LRFD Bridge Design Specifications*, 10<sup>th</sup> ed., American Association of State Highway and Transportation Officials, Washington, DC.
- AISC (2022). *Specification for Structural Steel Buildings*, American Institute of Steel Construction Chicago, IL.
- Adams, P.F., Lay, M.G. and Galambos, T.V. (1964). "Experiments on high strength steel members," Fritz Engineering Laboratory Report No. 297.8, 71 pp
- ASCE (2022). *Minimum Design Loads and Associated Criteria for Buildings and Other Structures*, ASCE 7-22, American Society of Civil Engineers, Washington, DC.
- Bartlett, F.M., Dexter, R.J., Graeser, M.D., Jelinek, J.J., Schmidt, B.J., and Galambos, T.V. (2003). "Updating Standard Shape Material Properties Database for Design and Reliability." *Engineering Journal*, 40 (1), 2–14.
- Boeraeve, P., Lognard, B., Janss, J., Gerardy, J.C., and Schleich, J.B. (1993). Elasto-plastic behaviour of steel frame works. *Journal of Constructional Steel Research*, 27(1-3), 3-21.
- CEN (2022). *Eurocode 3 – Design of Steel Structures – Part 1-1: General Rules and Rules for Buildings*, EN 1993-1-1, Comité Européen de Normalisation, Brussels.
- ConSteel (2025). [consteelsoftware.com](https://consteelsoftware.com), accessed Feb. 9, 2025.
- Dibley, J. E. (1970). "A preliminary investigation into the use of high-strength structural steel in structures designed plastically" (No. EG/A/13/70).
- Dibley, J. E. (1969). "Lateral torsional buckling of I-sections in grade 55 steel," *Proceedings of the Institution of Civil Engineers*, 43(4), 599-627.
- Driscoll, G.C. and Beedle, L.S. (1957). "The Plastic Behavior of Structural Members and Frames," *The Welding Journal*, 36(6), 275-286.
- Dux, P.F., and Kitipornchai, S. (1983). "Inelastic beam buckling experiments," *Journal of Constructional Steel Research*, 3(1), 3-9.
- Eetikala, A.R. (2025). "Experimental database for lateral-torsional and flange local buckling of rolled I-section members," Structural Engineering Mechanics and Materials Report 2025-25, School of Civil and Environmental Engineering, Georgia Institute of Technology, Atlanta, GA.
- El Darwish, I. A., and Johnston, B. G. (1965). Torsion of structural shapes. *Journal of the Structural Division*, 91(1), 203-227.
- Ellingwood, B.E., Galambos, T.V., MacGregor, J.G., and Cornell, C.A. (1980). *Development of a Probability Based Load Criterion for American National Standard A58*, NBS Publication No. 577, 219 pp.

- Ellingwood, B.E., MacGregor, J.G., Galambos, T.V., and Cornell, C.A. (1982). "Probability-Based Load Criteria: Load Factors and Load Combinations." *Journal of the Structural Division*, 108(5), 978–997.
- Fukumoto, Y., and Kubo, M. (1977). "An Experimental Review of Lateral Buckling of Beams and Girders," *Stability of Structures Under Static and Dynamic Loads*, ASCE, 541– 562.
- Galambos, T.V. (2004). "Reliability of the Member Stability Criteria in the 2005 AISC Specification." *Steel Structures*, 4, 223-230.
- Galambos, T.V., Ellingwood, B.E., MacGregor, J.G., and Cornell, C.A. (1982). "Probability-Based Load Criteria: Assessment of Current Design Practice," *Journal of the Structural Division - ASCE*, 108(5), 959-977.
- Galambos, T.V. and Ravindra, M.K. (1976). Tentative Load and Resistance Factor Design Criteria for Steel Plate Girders, Progress Report to the Advisory Committee of AISI Project 163 "Load Factor Design of Buildings," Research Report No. 29, Structural Division, Department of Civil Engineering, School of Engineering and Applied Science, Washington Univ., St. Louis, MO, 42 pp.
- Greiner, R., and Kaim, P. (2001). "Comparison of LT-buckling curves with test results," Report No. 2001-004; 23, ECCS TC8.
- Greiner, R., Salzgeber, G., and Ofner, R. (2000). "New Lateral Torsional Buckling Curves  $\kappa_{LT}$  - Numerical Simulations and Design Formulae," ECCS TC8, Report 30, June 2000 (rev), European Convention for Constructional Steelwork, Brussels, Belgium.
- Janss, J., and Massonnet, C. (1967). "The extension of plastic design to steel A52." *Publications of the IABSE*, 27, 15-30.
- Kemp, A.R. (1996). "Inelastic local and lateral buckling in design codes," *Journal of Structural Engineering*, 122(4), 374-382.
- Kemp, A.R. (1986). "Factors affecting the rotation capacity of plastically designed members," *The Structural Engineer*, 64B(2), 28-35.
- Knobloch, M., Bureau, A., Kuhlmann, U., Simões da Silva, L., Snijder, H.H., Taras, A., and Jörg, F. (2020). "Structural member stability verification in the new Part 1 - 1 of the second generation of Eurocode 3: Part 2: member buckling design rules and further innovations." *Steel Construction*, 13(3), 208-222.
- Kusuda, T., Sarubbi, R.C., and Thurlimann, B. (1960). "Bracing of beams in plastically designed steel structures." Lehigh University. Lehigh Preserve Institutional Repository. <https://preserve.lehigh.edu>.
- Lee, G. C., Ferrara, A. T., Galambos, T. V., and Lay, M. G. (1964). *Experiments on braced wide-flange beams*. Welding Research Council.
- Lee, G.C., and Galambos, T.V. (1962). "Post-buckling strength of wide-flange beams," *Journal of the Engineering Mechanics Division*, 88(1), 59-75.
- Lukey, A.F., Smith, R.J., Hosain, M.U. and Adams, P.F. (1969). "Experiments on Wide-Flange Beams under Moment Gradient," *Welding Research Council Bulletin*, 142, 1-19.
- McDermott, J.F. (1969). "Plastic bending of A514 steel beams." *Journal of the Structural Division*, 95(9), 1851-1871.
- Prasad, J., and Galambos, T.V. (1963). "The influence of the adjacent spans on the rotation capacity of beams," Fritz Engineering Laboratory, Department of Civil Engineering, Lehigh University.
- Phillips, M.L., Slein, R., Sherman, R.J., and White, D.W. (2024a). "Proposed Improvements to AISC 360-22 for Built-Up I-Section Members," *Journal of Constructional Steel Research*, Vol. 217, <https://doi.org/10.1016/j.jcsr.2024.108657>.
- Phillips, M., Slein, R., Sherman, R.J., and White, D.W. (2024b). "Experimental Database for Lateral-Torsional Buckling of Built-Up I-Section Members," *Mendeley Data*, V1, doi: 10.17632/v2pr9rbxyk.1.
- Sawyer, H. A. (1961). Post-elastic behavior of wide-flange steel beams. *Journal of the Structural Division*, 87(8), 43-71.
- Slein, R., Kamath, A.M., Phillips, M., Toğay, O., Sherman, R.J., and White, D.W. (2024). "Flexural Resistance of Thin-Web Singly-Symmetric Steel I-Section Members Exhibiting Early Tension Flange Yielding." *Journal of Constructional Steel Research*, 221, <https://doi.org/10.1016/j.jcsr.2024.108831>.
- Subramanian, L., and White, D.W. (2017). "Reassessment of the lateral torsional buckling resistance of rolled I-section members: moment gradient tests." *Journal of Structural Engineering*, 143(4), 04016203.
- Subramanian, L., Jeong, W.Y., Yellepeddi, R., and White, D.W. (2018). "Assessment of I Section Member LTB Resistances Considering Experimental Test Data and Practical Inelastic Buckling Design Calculations." *Engineering Journal*, AISC, 55, 15–44.
- Suzuki, T., and Kubodera, M. (1973). "Inelastic lateral buckling of steel beams" *Annual Meeting of Architectural Institute of Japan*, Tokyo.
- Suzuki, T., and Ono, T. (1970a). Experimental study of inelastic beams (1) - Beam under uniform moment, *Transactions of the Architectural Inst. of Japan*, 168, 77-84.

- Suzuki, T., and Ono, T. (1970b). Experimental study of inelastic beams (2) - Beam under moment gradient, *Transactions of the Architectural Inst. of Japan*, 45(171), 31-36.
- Suzuki, T. and Ono, T. (1970c). "Experimental Study of Inelastic Beams (3) – Beam Bracing on the Both Sides of Plastic Hinge," *Transactions of the Architectural Institute of Japan*, 45(175) (in Japanese), 69-74.
- Taras, A., and Greiner, R. (2010). "New design curves for lateral–torsional buckling—Proposal based on a consistent derivation," *Journal of Constructional Steel Research*, Vol 66, pp. 648-663, <https://doi.org/10.1016/j.jcsr.2010.01.011>.
- Taras, A., and Greiner, R. (2008). Development of consistent buckling curves for torsional and lateral-torsional buckling. *Steel Construction: Design and Research*, 1(1), 42-50.
- Udagawa, K., Saisho, M., Takanashi, K., and Tanaka, H. (1973). "Experiments on lateral buckling of H-shaped beams subjected to monotonic loadings," *Transactions of the Architectural Institute of Japan*, 212, 23-36.
- Wakabayashi, M., Nakamura, T., and Okamura, N. (1970). "Studies on lateral buckling of wide flange beams (1)." *Disaster Prevention Research Institute Annuals*, 14.
- White, D.W., and Vaszilievits-Sömjén, B. (2025). "Practical stability design of I-section members for combined forces," *Annual Stability Conference*, Structural Stability Research Council, April, to appear.
- White, D.W., Jeong, W.Y., and Slein, R. (2021a). *Frame Design Using Nonprismatic Members, Design Guide 25*, 2nd Edition, American Institute of Steel Construction Chicago, IL, and Metal Building Manufacturers Association, Cleveland, OH, dedicated in memory of R. Kaehler and Y.D. Kim.
- White, D.W., Toğay, O., Slein, R. and Jeong, W.Y. (2021b). "SABRE2-V2". <http://white.ce.gatech.edu/sabre>.
- White, D.W. (2008). "Unified Flexural Resistance Equations for Stability Design of Steel I-Section Members – Overview," *Journal of Structural Engineering*, ASCE, 134(9), 1405-1424.
- White, D.W., and Kim, Y.D. (2008). "Unified flexural resistance equations for stability design of steel I-section members: moment gradient tests," *Journal of Structural Engineering*, 134(9), 1471-1486.
- White, D.W., and Jung, S.K. (2008). "Unified flexural resistance equations for stability design of steel I-section members: uniform bending tests," *Journal of Structural Engineering*, 134(9), 1450-1470.
- Wong, E. and Driver, R. (2010), "Critical evaluation of equivalent moment factor procedures for laterally unsupported beams," *Engineering Journal*, AISC, 47(1), 1–20 and Closure, 47(4), 281–283.
- Wong-Chung, A.D., and Kitipornchai, S. (1987). "Partially braced inelastic beam buckling experiments," *Journal of Constructional Steel Research*, 7(3), 189-211.
- Yura, J.A., Galambos, T.V. and Ravindra, K. (1978), "The Bending Resistance of Steel Beams," *Journal of the Structural Division*, ASCE, 104(ST9), 1355-1369.
- Ziemian, R.D. (Ed.) (2010). *Guide to Stability Design Criteria for Metal Structures*, 6th Edition, John Wiley and Sons, Inc., Hoboken, NJ.